Morphologies and Energies of Néel Inversion Wall Defects in a Liquid Crystal Polyether

Mary Jane E. O'Rourke, Ding-Kuo Ding, and Edwin L. Thomas*

Departments of Materials Science and Engineering and Chemical Engineering, Massachusetts Institute of Technology, Cambridge, Massachusetts 02139

Virgil Percec

Department of Chemistry, University of Pennsylvania, Philadelphia, Pennsylvania 19104

Received April 11, 2001; Revised Manuscript Received June 20, 2001

ABSTRACT: Two-dimensional Néel inversion walls formed in a nematic monodomain during magnetic realignment of a highly elastically anisotropic thermotropic liquid crystal polyether ($\epsilon \approx +0.5$; $k_{11} \approx 3k_{33}$) are examined via polarized light microscopy (PLM). The detailed director patterns of these walls are then imaged at high resolution by atomic force microscopy (AFM) through a lamellar decoration technique, employed after the walls have been fixed by quenching while under a field. Walls form as closed loops composed of a continuous inversion wall with antiparallel director alignment of the interior region with respect to that of the exterior. The energy of Néel walls is theoretically evaluated as a function of elastic anisotropy, and it is shown that, in the extreme of $\epsilon = +1.0$, indicating easy bend distortion, a Néel bend wall is 58% lower in energy than a Néel splay wall. Correspondingly, for easy splay distortion, i.e., $\epsilon = -1.0$, the situation reverses. In our experimental system, the energy of a splay wall is 17% higher than that of a bend wall. The variation of the characteristic width of the walls in this polyether as measured by AFM yields an effective elastic constant of 1.6×10^{-6} dyn at 160 °C. Inversion wall dynamics can be followed through time-under-field experiments. Loops coalesce, shrink, and smooth their curvature, occasionally splitting into partial loops terminated by two opposite-strength $^1/_2$ disclinations. The observed more rapid shrinkage of splay-distortion-rich wall segments as compared to that of bend-rich wall segments corresponds to the wall energetics expected on the basis of the elastic anisotropy of the polymer.

Introduction

The distortional free energy of a nematic liquid crystal in a magnetic field is composed of a gradient elastic term and a nonlinear magnetic term, as given in eq 1

$$g = \frac{1}{2}[k_{11}(\nabla\cdot\mathbf{n})^2 + k_{22}(\mathbf{n}\cdot\nabla\times\mathbf{n})^2 + k_{33}(\mathbf{n}\times\nabla\times\mathbf{n})^2] - \frac{1}{2}\chi_a(\mathbf{n}\cdot\mathbf{H})^2 \quad (1)$$

where **n** is a nonpolar unit vector describing the liquid crystal director. The elastic term was formulated by Frank as an expansion of gradients in the director field, where k_{11}, k_{22}, and k_{33} are the Frank elastic constants for the three independent modes of distortion: splay, twist, and bend, respectively.[1] The magnetic term takes into account the magnetic field strength, H, and the diamagnetic susceptibility anisotropy, χ_a. The diamagnetic susceptibility anisotropy is the difference between the susceptibility of the molecules to parallel alignment with a magnetic field, $\chi_{||}$, and to perpendicular alignment with the field, $\chi_\perp$; $\chi_a = \chi_{||} - \chi_\perp$. Thus, χ_a determines the orientation of the director with respect to the field. When $\chi_a > 0$, the director aligns parallel (or antiparallel) to the field. The elastic and magnetic terms balance each other, with the elastic term dispersing distortions and the magnetic term globally orienting the director and localizing distortions. The lowest energy state is the monodomain, the defect-free state of the liquid crystal, with uniform alignment of the director along the magnetic field.

* Author to whom correspondence should be addressed.

When an external field is applied orthogonal to the director of a monodomain, the director reorients by 90°, with regions aligning either parallel or antiparallel to the field. Characteristic inversion walls form, separating the regions of parallel and antiparallel alignment. The director undergoes a rotation of π from one side of the wall to the other. Inversion walls can be formed in nematic liquid crystals during director reorientation via flow, electric, or magnetic fields.[2−6] The three types of director distortions possible in nematic liquid crystals, splay, twist, and bend, give rise to three different inversion wall distortions, first characterized by Helfrich.[7] The wall defects that form in a nematic liquid crystal are analogous to Bloch walls (pure twist distortions) or Néel walls (a combination of splay and bend distortions) in magnetic spin systems.[7]

In a thin-film liquid crystal sample, it is reasonable to assume that the director is confined to lie in the plane of the film and that twist distortions do not occur. With only in-plane distortions permitted, walls containing only bend and splay distortions are formed when an in-plane magnetic field is applied perpendicular to the monodomain director. Bend is the primary mode of distortion in bend−splay Néel walls that form parallel to the applied field (Figure 1A), and splay is the primary mode of distortion in splay−bend Néel walls that form perpendicular to the field (Figure 1B). Isolated Néel walls have mirror symmetry. Henceforth, we shall refer to the two types of Néel walls by their primary mode of distortion in this paper, i.e., Néel splay and Néel bend, noting that both modes of distortion are present in each.

When the elastic contribution to the distortional free energy is considered, the Frank elastic constants for splay, twist, and bend distortions are often assumed to

10.1021/ma010635y CCC: $20.00
Published on Web 08/07/2001

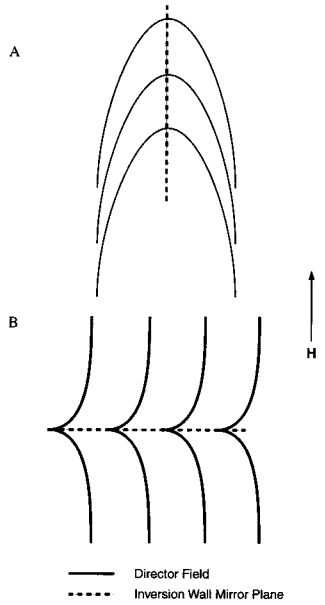

Figure 1. (A) Bend−splay wall, analogous to a Néel wall in magnetic spin systems. The primary mode of distortion is bend. This wall forms parallel to the field. Isolated walls have mirror symmetry. (B) Splay−bend wall perpendicular to the field, where the primary mode of distortion is splay. Again, isolated walls have mirror symmetry.

be equivalent ($k_{11} = k_{22} = k_{33}$). The equiconstant approximation is often reasonable for small molecule liquid crystals (SMLCs), but rarely is it appropriate for liquid crystal polymers (LCPs) because of their strong elastic anisotropy. In the two-dimensional thin-film geometry, the elastic anisotropy, ϵ, for splay and bend distortions can be defined as

$$\epsilon = \frac{k_{11} - k_{33}}{k_{11} + k_{33}} \tag{2}$$

Previous Experimental Observations of Walls

The detailed structure of both Néel splay and bend walls has not been extensively investigated in small molecule liquid crystals (SMLCs) or liquid crystal polymers (LCPs).[1] Inversion walls are topologically constrained to loop upon themselves or to end at surfaces or disclinations.[2,5,6,9,10] In contrast to wall defects, disclinations are rotational symmetry-breaking defects and can be point or line defects. The strength of a disclination is equal to the number of rotations the director experiences on a path encircling the disclination.

Williams, Vitek, and Kléman observed surface disclination lines in the small molecule liquid crystal, MBBA, confined between two rubbed glass plates twisted with respect to each other.[11] The proposed director pattern of such a surface disclination line loop lying in the plane of its confining boundary corresponds very well to the experimental director patterns of the wall loops imaged in the liquid crystal polymer studied in the present work. Kléman et al. remark that these surface lines can also be considered as the emergence of a wall essentially of Néel character at the surface of the film.

Stieb et al. have used polarized light microscopy to study the structure of twist walls formed in small molecule liquid crystals during realignment by an electric field.[6] They observed shrinkage of closed loops and breakage of closed loops into wall segments terminated by a pair of disclination lines. Rey proposed a model for the shrinkage of a Néel bend−splay inversion wall segment and its subsequent disappearance via the annihilation of the terminating $\pm 1/2$ disclination line pair.[12] The velocity of a disclination line as it follows the path of the shrinking wall scales with the inverse of the thickness of the wall that it terminates. Additionally, the model predicts that higher strength disclinations move more slowly, as they involve stronger director distortions. Rojstaczer and Stein demonstrated that the disclination density in both a rigid and a semiflexible polyester is proportional to $\gamma_{\text{eff}}/k_{\text{eff}}$, where γ_{eff} is an effective viscosity coefficient, although the time scale of the domain growth process for the rigid polyester was over 2 orders of magnitude slower than that for the flexible polyester.[13]

Léger observed elliptical twist−bend wall loops created in MBBA via a Frederiks transition induced by a magnetic field.[5] During shrinkage, isolated closed loop inversion walls were observed to attain a fixed ellipticity. For SMLCs, twist is the easiest deformation mode. Léger determined elastic constant ratios in MBBA from the ellipticity of the inversion wall loops and found $\sqrt{(k_{11}/k_{22})} = 1.45$ and $\sqrt{(k_{33}/k_{22})} = 1.7$. These values give an elastic anisotropy of $\epsilon = -0.16$ for MBBA, with $k_{33} \approx 3k_{22}$ and $k_{11} \approx 2k_{22}$.

LCPs typically have strong elastic anisotropy. Theory predicts that the bend elastic constant increases linearly with persistence length, but that the splay constant is proportional to chain length.[14] In a main chain thermotropic LCP, a splay deformation requires free chain ends. Because the presence of chain ends in a high molecular weight polymer sample is minimal, a large Frank elastic constant for splay, k_{11}, is expected. However, if the polymer chains are sufficiently flexible, hairpin defects (localized π turns in the chain backbone) can function similarly to chain ends and lower the effective splay constant. Polydispersity of the polymer can also alter elastic constants.[15,16] Typically, the splay constant is found to be much higher than the constants for twist or bend distortions in polymers ($k_{11} > k_{22} \approx k_{33}$). Hudson and Thomas analyzed the director field patterns in images of disclinations to determine the elastic anisotropy of two polyesters.[17] They found $\epsilon = -0.4$ for a rigid polymer, indicating a large contribution from bend distortion, whereas for a flexible-chain thermotropic LCP, $\epsilon = 0.1$. These values are valid at 100 nm from a disclination core and were obtained by fitting director angles on a circuit about $+1/2$ disclinations, measured at the fixed radius from the core. Asymptotic values of the elastic anisotropy, ϵ_a, were evaluated at distances far from the disclination core (1 μm) and found to be $\epsilon_a \approx 0$ for the rigid polymer and $\epsilon_a \approx -0.15$ for the flexible polymer. The significant radial dependence of elastic anisotropy reflects the large distortions that take place at a disclination core.[17] Hudson and Thomas also observed Néel bend inversion wall segments in a liquid crystal polyester, formed between preexisting $+1/2$ and $-1/2$ disclinations when placed in a magnetic field.[2] Figueiredo Neto et al. computed the director texture of a Néel bend wall with a twist deformation perturbation, assuming $k_{22} = k_{33} = \alpha k_{11}$, with $\alpha \ll 1$. The model predicts that the ellipticity of closed loop inversion walls in polymer nematics would be approximately two times greater than that suggested by Léger for SMLCs because of the high contribution of splay to the elastic distortional free energy, in combination with the viscous drag effects present in polymer liquid crystals.[18]

Table 1. Influence of Elastic Anisotropy on Néel Wall Energy

elastic anisotropy	Néel bend wall energy[a]	Néel splay wall energy[a]
1	1.00	1.58
0.5	1.24	1.52
0	1.42	1.42
−0.5	1.52	1.24
−1	1.58	1.00

[a]Values are normalized with respect to the energy of a Néel bend wall, $[(k_{11} + k_{33})\chi_a H^2]^{1/2}$.

In this paper, we first calculate the energies of splay and bend Néel inversion walls as functions of k_{11} and k_{33}. We then determine k_{eff}, an effective equiconstant-approximate elastic constant, for our liquid crystal polyether by measuring the characteristic Néel inversion wall width, ξ_{wall}, as a function of the strength of the applied magnetic field. We observe experimentally the morphology of splay and bend Néel inversion walls over their evolution. Inversion walls are readily observed via polarized light microscopy (PLM). The detailed director trajectories across the two types of Néel inversion walls in this geometry can be directly visualized via either atomic force microscopy (AFM) or high resolution scanning electron microscopy (HRSEM) using the lamellar decoration technique, a technique applicable to crystallizable thermotropic LCPs.[2,7] Inversion wall evolution can be monitored by repeatedly holding the sample in an applied field for intervals of time, quenching, and examining the director texture by AFM after each increment. The observed evolutions of the two types of inversion walls in this experiment are commensurate with their calculated energy difference.

Modeling of the Director Pattern of Néel Walls

The director in a liquid crystal sample can be confined to lie in the plane of the film if the thickness, h, is small. Substantial twist distortions are not possible, and the director has only one degree of freedom, ϕ, the angle with respect to a fixed axis within the plane. The distortional free energy density can therefore be described by considering only the splay and bend elastic constants. Assuming that the director is confined to the xy plane and that the field is along the y direction such that $\phi_h = 0$, the free energy density can be written as

$$g = \frac{1}{2}\left[(k_{11}\cos^2\phi + k_{33}\sin^2\phi)\left(\frac{\partial\phi}{\partial x}\right)^2 + (k_{11}\sin^2\phi + k_{33}\cos^2\phi)\left(\frac{\partial\phi}{\partial y}\right)^2 + 2(k_{33} - k_{11})\sin\phi\cos\phi\left(\frac{\partial\phi}{\partial x}\right)\left(\frac{\partial\phi}{\partial y}\right)\right] - \frac{1}{2}\chi_a(\mathbf{n}\cdot\mathbf{H}) \quad (3)$$

The total free energy of the system is

$$G = \int_0^h \int\int g(x,y)\,dx\,dy\,dz \quad (4)$$

Helfrich minimized the total free energy, G, and found the structure of inversion walls for the case of equivalent elastic constants.[7] We have taken elastic anisotropy into account for the solution of the general and specific cases of the structure of both bend-rich and splay-rich Néel walls, assuming that the director distortions depend only on distance from the wall.[19] By minimizing the expression for the free energy, the director field can be solved in terms of this elastic anisotropy. With elastic anisotropy taken into account, it follows that the distortional energies for the two types of Néel walls will be different because of their dissimilar director distortions. One thus anticipates a differential rate of elimination of each type of wall distortion during realignment in a magnetic field.

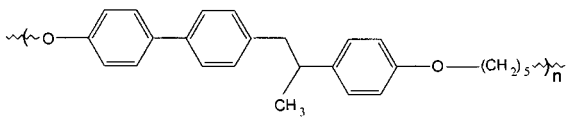

Figure 2. Semi-flexible main chain liquid crystal polyether that exhibits a melting temperature of 148 °C and a nematic-to-isotropic transition temperature of 183 °C. This crystallizable polymer has a glass transition temperature of 70 °C, and thus, its director field can be visualized by the lamellar decoration technique.

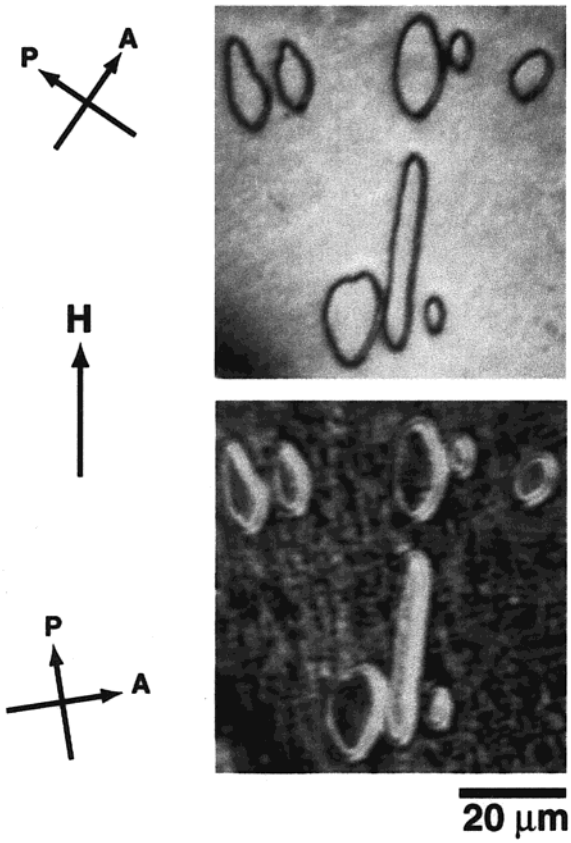

Figure 3. (A) PLM images of inversion wall loops where the magnetic field direction is oriented at 45° to the polarizer and analyzer. Most of the sample appears bright, as the birefringent liquid crystal alters the polarization of light, enabling it to pass through the analyzer. Wall loops appear as two parallel extinction contours. Both elliptical and irregularly shaped inversion wall loops are visible. (B) PLM images of inversion wall loops where the magnetic field direction is oriented parallel to the polarizer and perpendicular to the analyzer. (The sample has been rotated by 45° from its original position in Figure 5A.) Extinction regions are obvious on both sides of the inversion walls, demonstrating that the molecules are well aligned along the magnetic field. The director of the monodomain is now parallel to the polarizer, the polarization of the incident light is unchanged, and the analyzer extinguishes all light. The sample appears bright only along Néel inversion walls, as all distortions are localized to these defects and the director is at some angle to the polarizer. A single dark line appears along the wall centerline. In this region of the wall defect, the director is exactly perpendicular to the magnetic field direction and therefore perpendicular to the polarizer, resulting in an extinction line.

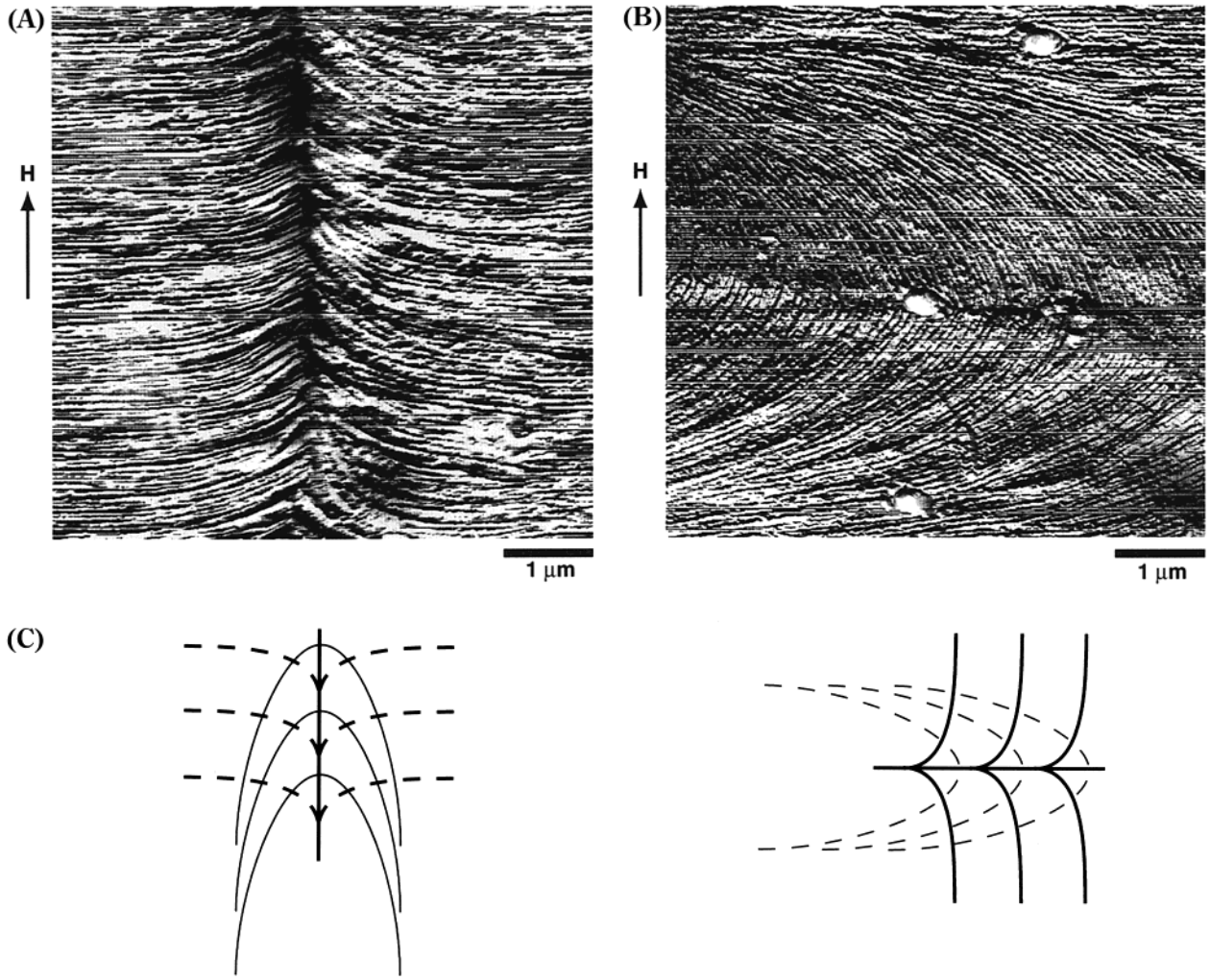

Figure 4. (A) AFM director field imaging of a bend wall via the lamellar decoration technique, with lamellae perpendicular to the director appearing as a splay wall. This wall is a straight portion of a large loop where opposite sides are noninteracting. (B) AFM image of a lamellar-decorated splay wall, with lamellae perpendicular to the director appearing as a bend wall. Note that the width of the wall in 4B is substantially greater than that in 4A, consistent with the relative values of the splay and bend elastic constants. (C) Lamellae are everywhere normal to the local director. A bend wall in the director field (solid lines) will appear as a splay wall (dashed lines) in the lamellae, while a splay wall in the director field (solid lines) will appear as a bend wall (dashed lines) in the lamellae.

An effective elastic constant (equiconstant approximation) can be obtained directly from images of a straight section of an inversion wall oriented approximately parallel or perpendicular to the magnetic field through measurement of the angle of the director with respect to the field direction as a function of distance from the center of the wall. With a known value of the magnetic susceptibility parameter, the absolute value of an effective Frank elastic constant can be determined.[3] If elastic anisotropy is considered in the solution of the director orientation across Néel walls, the elastic anisotropy of the LCP can be determined through its variation in numerical solutions of director orientation and selection of the solution that best fits the imaged director field.[20] The appropriate characteristic length is redefined by replacing the effective elastic constant with the sum of the splay and bend constants. Using this new characteristic length and a known value of the magnetic susceptibility parameter, the absolute values of the Frank elastic constants for splay and bend, k_{11} and k_{33}, can be determined.

Interactions between adjacent inversion walls were considered by de Gennes for small-molecule liquid crystals.[21] The potential energy between two parallel inversion walls in the case of equivalent elastic constants can be described as

$$U = U_0 + 4\chi_a H^2 \exp(-2d/\xi) \tag{5}$$

where $2d$ is the distance between the walls. The force that one inversion wall exerts on the other is

$$f = 4H(k/\chi_a)^{1/2} \exp[-2dH/(k\chi_a)^{1/2}] \tag{6}$$

The interaction of inversion walls in a material with elastic anisotropy is still to be described.

Energy of Néel Walls. Elastic anisotropy influences the relative energy of the various types of inversion walls and the wall dynamics. In this section, we develop the general form of the wall energy for both the bend-rich and splay-rich Néel walls in a nematic with elastic anisotropy.

The inversion wall energy per unit area of wall of height h and length l, G/hl, was first derived by Helfrich[8] for a wall with equivalent elastic constants

$$\frac{G}{hl} = 2H(\chi_a k)^{1/2} \tag{7}$$

This wall energy expression indicates that the change in the total wall energy is simply proportional to the change in the total wall length. The force causing an isolated inversion wall to shrink is thus independent of wall length. Therefore, the rate of wall shrinkage, either from shrinkage of a wall loop or from the movement of disclinations along the wall, is constant at a specific condition, i.e., fixed field strength or temperature (which influences elastic constants).

For a nematic with elastic anisotropy, the energy per unit area of a two-dimensional Néel bend wall can be derived from eqs 3 and 4 as

$$\frac{G}{hl} = \int_{\infty}^{-\infty} \frac{1}{2}(k_{11}\cos^2\phi + k_{33}\sin^2\phi)\left(\frac{\partial\phi}{\partial x}\right)^2 \mathrm{d}x - \int_{\infty}^{-\infty} \frac{1}{2}\chi_a(\mathbf{n}\cdot\mathbf{H})^2 \mathrm{d}x \quad (8)$$

where ϕ is a function of x only. Similarly, the energy per unit area of the Néel splay wall, where ϕ is a function of y only, is given by

$$\frac{G}{hl} = \int_{\infty}^{-\infty} \frac{1}{2}(k_{11}\sin^2\phi + k_{33}\cos^2\phi)\left(\frac{\partial\phi}{\partial x}\right)^2 \mathrm{d}x - \int_{\infty}^{-\infty} \frac{1}{2}\chi_a(\mathbf{n}\cdot\mathbf{H})^2 \mathrm{d}x \quad (9)$$

In the general case, the energy of the Néel bend wall can be rewritten as

$$\frac{G}{hl} = \frac{k}{2\xi}\int_{\infty}^{-\infty} \frac{1}{2}[(1+\epsilon)\cos^2\phi + (1-\epsilon)\sin^2\phi]\left(\frac{\partial\phi}{\partial x'}\right)^2 \mathrm{d}x' - \int_{\infty}^{-\infty} \frac{1}{2}\chi_a(\mathbf{n}\cdot\mathbf{H})^2 \mathrm{d}x \quad (10)$$

and the energy of the Néel splay wall as

$$\frac{G}{hl} = \frac{k}{2\xi}\int_{\infty}^{-\infty} \frac{1}{2}[(1-\epsilon)\sin^2\phi + (1+\epsilon)\cos^2\phi]\left(\frac{\partial\phi}{\partial x'}\right)^2 \mathrm{d}x' - \int_{\infty}^{-\infty} \frac{1}{2}\chi_a(\mathbf{n}\cdot\mathbf{H})^2 \mathrm{d}x \quad (11)$$

where $k = (k_{11} + k_{33})/2$ is the mean elastic constant, $\epsilon = (k_{11} - k_{33})/(k_{11} + k_{33})$ is the elastic anisotropy as in eq 2, $\zeta = [(k_{11} + k_{33})/\chi_a H^2]^{1/2}$ is defined as the characteristic magnetic coherence length for a two-dimensional Néel inversion wall, and $x' = x/\zeta$ is the dimensionless distance along the normal to the wall. Numerical integration of eqs 10 and 11 yields the values of the energies of Néel bend and splay walls for different values of elastic anisotropy (see Table 1). Examining the table, we see that, in the case of easy bend distortion ($\epsilon = +1.0$), a Néel bend wall is 58% lower in energy than a Néel splay wall. Correspondingly, for easy splay distortion, i.e., $\epsilon = -1.0$, the situation reverses.

Using the elastic constant values at 160 °C of $k_{11} = 2.8 \times 10^{-6}$ dyn and $k_{33} = 0.9 \times 10^{-6}$ dyn (previously determined from an analysis of the director distribution across Néel walls of this polyether LCP) and assuming a value of 1×10^{-7} emu ccgs for χ_a,[1] the Néel bend wall has an energy per unit area of 0.105 erg/cm^2, and a Néel splay wall has an energy per unit area of 0.123 erg/cm^2. The Néel splay wall energy is 17% higher than the energy for Néel bend walls, so the splay walls in the system will be the less energetically favorable distortion. The difference in the emergence and evolution behaviors of splay and bend inversion walls experimentally observed in the next section is in keeping with the general energy difference between splay and bend distortions arising from $k_{11} \approx 3k_{33}$.

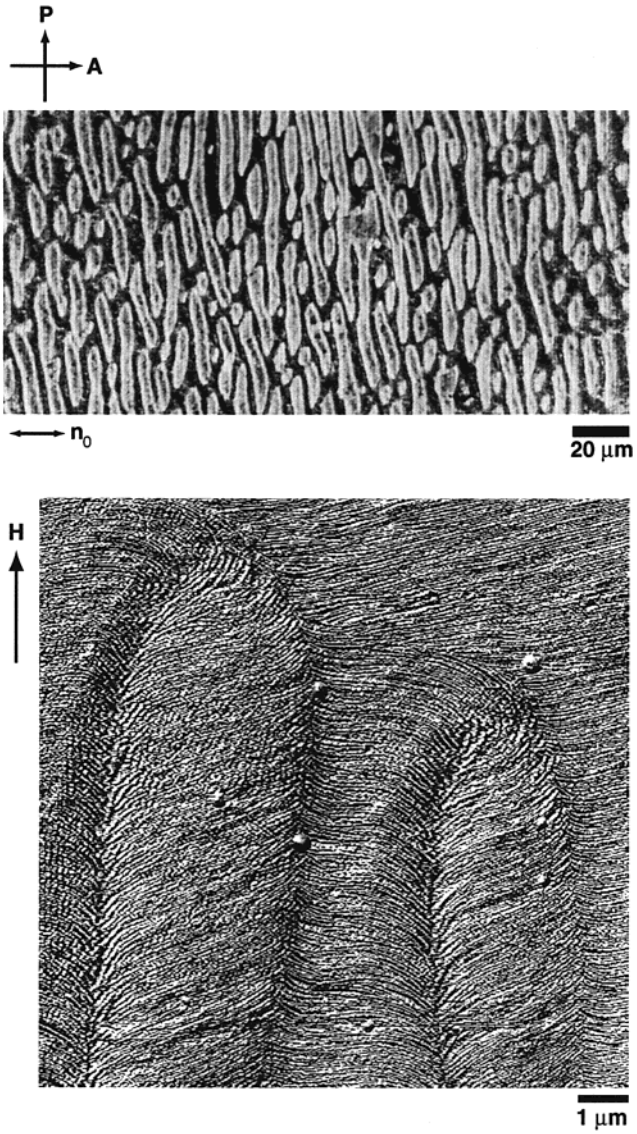

Figure 5. (A) Polarized light micrograph of transient textures at short times in the magnetic field. This texture forms as the director field of the monodomain first begins to reorient, prior to the development of well-defined Néel inversion walls. (B) High-resolution AFM image showing the tops of two loops of incomplete inversion walls in the transient texture pictured in Figure 4A. In the direction of the periodicity, developing Néel bend walls along the sides of the transient loops are imaged, with developing Néel splay walls at the tops of the transient loops. Note the opposing senses of the bend distortion of adjacent incomplete walls, resulting in the tops of the two loops having splay distortion of the same sense.

Experimental Section

The polymer investigated is a semiflexible main chain liquid crystal polyether obtained by the phase-transfer-catalyzed polyetherication of 1-(4-hydroxy-4′-biphenyl)-2-(4-hydroxyphenyl)propane with 1,5-dibromopentane (Figure 2).[18] This LCP has a positive diamagnetic susceptibility anisotropy, and thus, its director aligns parallel to the magnetic field direction. The number-average molecular weight is 11 200, and the polydispersity is 2.5, using THF−GPC−polystyrene standards. The phase behavior was determined by DSC at a heating rate of 20 °C/min and by wide and small angle X-ray scattering.

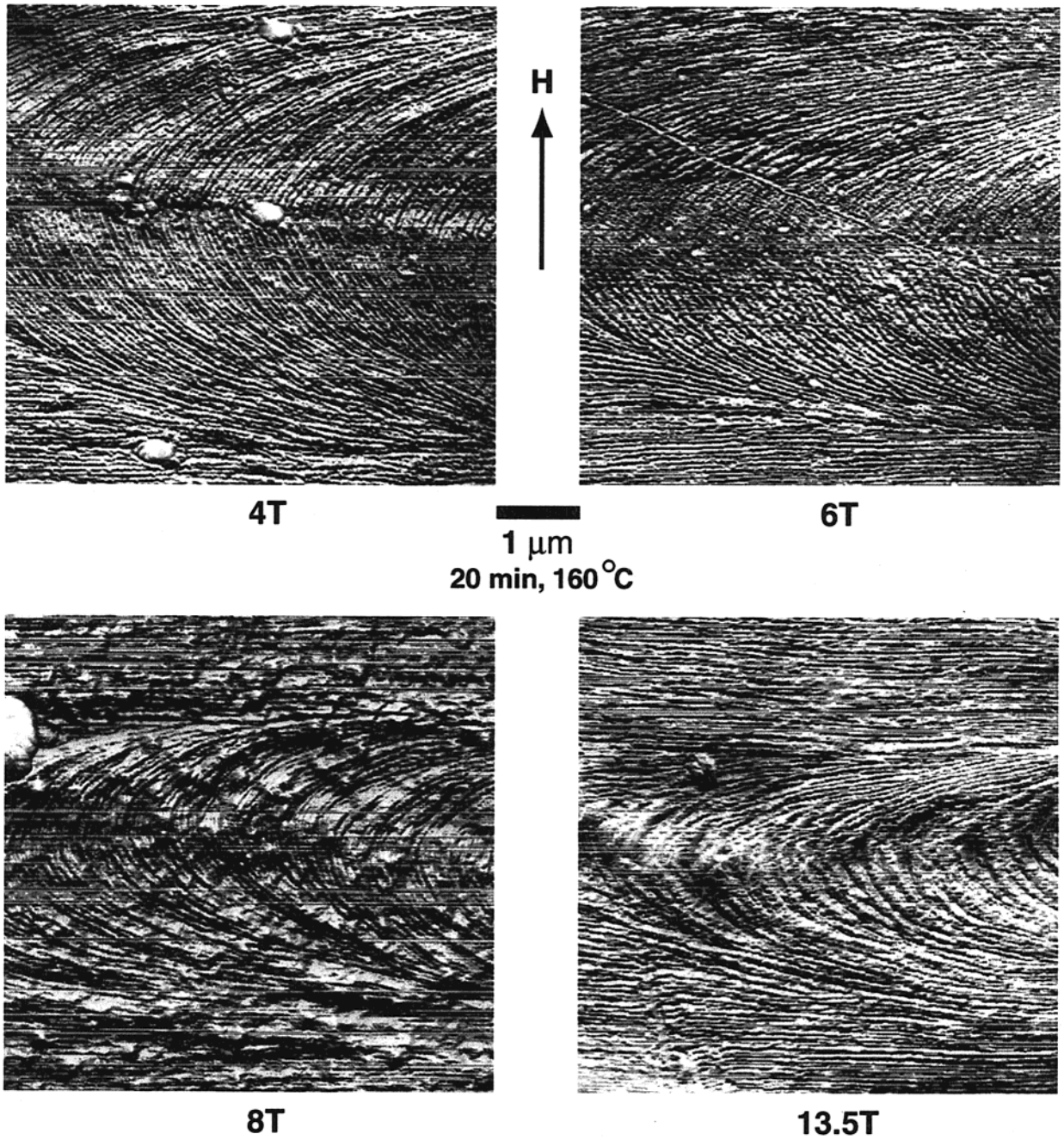

Figure 6. Magnetic field effect on inversion wall width. Walls were formed in fields of 4, 6, 8, and 13.5 T, all at 160 °C and after 20 min in the field. These four AFM images of Néel splay−bend walls are taken at the same magnification and clearly show that, as expected, an increase in field strength results in distortion localization to a decreasing characteristic width.

On heating, the glass transition temperature is 48 °C. The polymer exhibits a melting temperature of 148 °C and a nematic-to-isotropic transition temperature of 183 °C. Upon cooling at a rate of 20 °C/min, the isotropic-to-nematic transition occurs at 173 °C, the nematic-to-crystal transition at 108 °C, and the glass transition at 39 °C. The crystalline state is a distorted hexagonal phase in which the repeat unit is an almost fully extended conformation. The detailed synthesis and characterization of this polymer are given in ref 19.

In preparation for reorientation in the magnetic field, samples are heated to the nematic liquid crystal regime and a 1−2 μm thin film of polymer is sheared onto a glass slide with a razor blade, which imposes some shear alignment. An essentially defect-free liquid crystal monodomain is then achieved by application of a magnetic field parallel to the shear direction in a furnace-equipped superconducting magnet, where the sample is heated well into the liquid crystal regime (160 °C) and then quenched below room temperature while under the field at a rate of approximately 10 °C/s with a flow of nitrogen gas. The sample is then removed, rotated by 90°, and reinserted into the furnace-equipped magnet, which is still under the field. The sample is reheated to the liquid crystal regime at 160 °C and held for an interval on the order of minutes while the director reorients and inversion walls form. The inversion wall structures are fixed by a cold nitrogen gas quench to room temperature before the sample is removed from the field. The global director pattern can be imaged via PLM, and local director distortions can be imaged via either AFM or HRSEM through lamellar decoration.[9] It is possible to monitor the evolutionary behavior of the walls and the associated director fields by exposing the sample to a sequence of short time increments in the magnetic field while held at a temperature within the liquid crystal regime, with each exposure followed by quenching and PLM and AFM imaging. AFM is a good technique for experiments on the evolution of the director field, as it is a nondestructive technique that

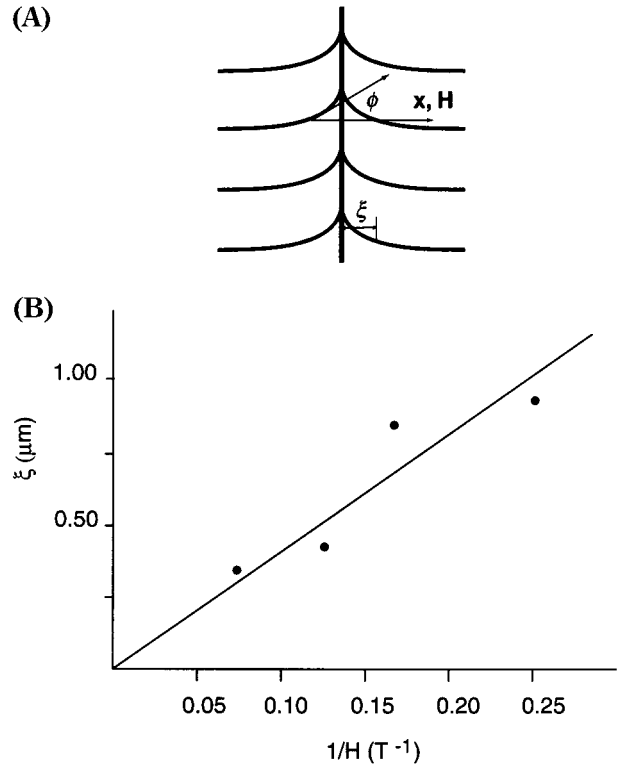

Figure 7. Characteristic width of alignment distortion, ξ, for each of the inversion walls in Figure 10 plotted versus the inverse of the strength of the magnetic field in which it was formed, $1/H$. ξ values are determined for each wall from the equation $\phi(x) = 2 \arctan[e^{(\pm\xi/x)}]$, where $\phi(x)$ is the angle that the director makes with respect to the field direction at a given distance from the center of the wall. $\phi(x)$ is measured directly from the high-resolution AFM images of the director of each wall.

requires no sample coating or etching, unlike SEM. AFM is also free of the electron beam-induced cross-linking and chain-scission damage that organic materials encounter in SEM.

It is through the introduction of height variation contrast that the lamellar decoration technique allows for high resolution AFM or SEM imaging of the director field of crystallizable thermotropic LCPs.[4] After the material is quenched from the nematic phase, it is annealed above the glass transition temperature, T_g, but below the crystal melting point, T_m. The liquid crystal polyether crystallizes slowly at room temperature due to the proximity of T_g. The resulting periodic fine-scale crystalline lamellae that form everywhere perpendicular to the director upon crystallization from the nematic state protrude slightly from the surface. As the lamellae are about 100 Å thick and spaced approximately 200 Å apart, the director field can be determined on the same length scale as the polymer molecule itself. Since the lamellae that decorate the director pattern are everywhere normal to the local director, a bend wall in the director field will appear as a splay wall in the lamellae and vice versa.

A Zeiss polarized light microscope was used to observe the samples at room temperature. AFM images obtained with a Digital Instruments Nanoscope III operated in contact mode to reveal high-resolution details of the director field. As the Nanoscope is equipped with an auxiliary light microscope, specific walls within larger areas previously imaged by PLM can be located, and the corresponding AFM images can be obtained. Identification of a wall for re-imaging to map inversion wall evolution for dynamic experiments is thus facilitated.

Results and Discussion

Néel Inversion Walls. Polarized light microscopy is commonly used to image defects in liquid crystals. The

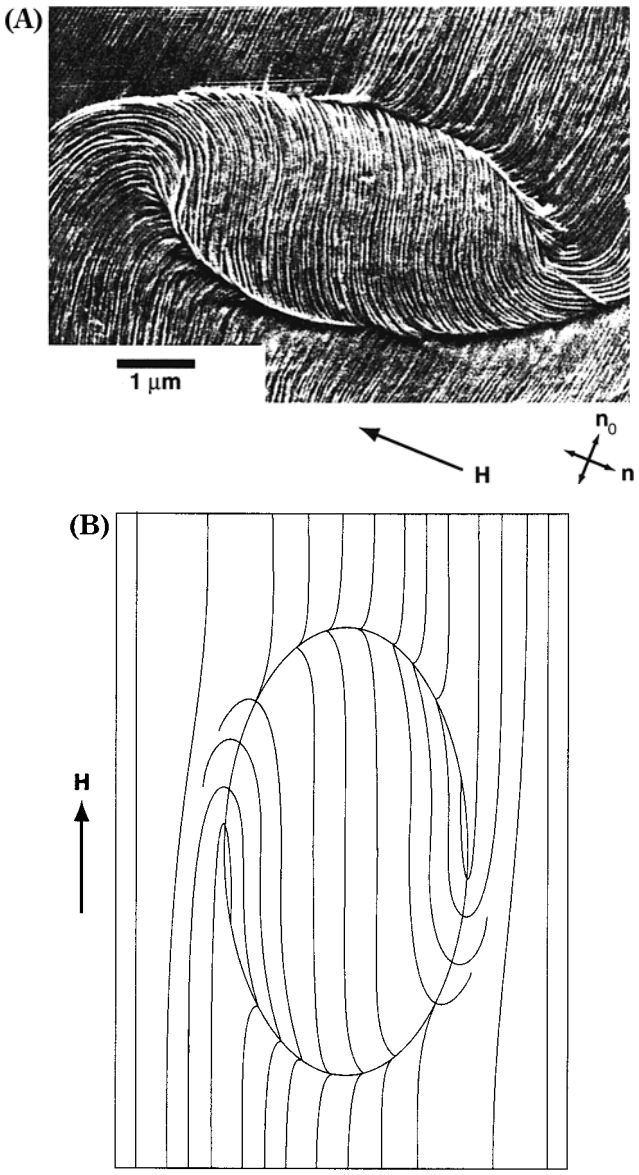

Figure 8. (A) High resolution SEM image of an inversion wall loop. Note the appearance of splay walls in the lamellae parallel to the field, indicating a bend wall in the director field, and bend walls in the lamellae perpendicular to the field, indicating splay walls in the director field. Note the gradual transition from Néel bend walls to Néel splay walls. (B) Schematic showing the director field of an elliptical wall loop and the continuous transitions from a bend wall segment oriented parallel to the field to a splay wall segment oriented perpendicular to the field.

appearance of Néel inversion walls in cross-polarized transmitted light can be understood as follows: If the liquid crystal has a positive diamagnetic anisotropy, the director serves as the local optical axis of the material. In regions where the director is either parallel or perpendicular to the plane of polarization of incident light, the polarization is unchanged by the material, and thus, the analyzer extinguishes the incident light. If a well-aligned sample is examined under PLM with the magnetic field direction at 45° to the polarizer (and at 45° to the analyzer), the sample will appear bright, as the birefringent liquid crystal rotates the polarization of light, enabling it to pass through the analyzer. Néel inversion walls will appear as two dark parallel lines. These extinction lines are the regions where the director is either parallel or perpendicular to the polarizer, and

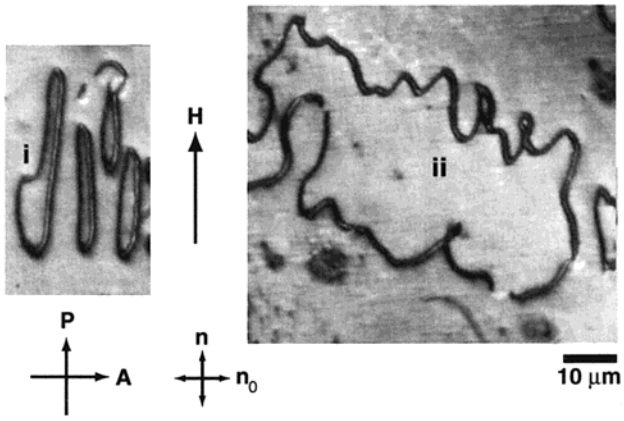

Figure 9. PLM micrographs of large and small irregularly shaped inversion wall loops. Note at position i that top-to-bottom coalescence of adjacent loops results in a new loop with an unusually large aspect ratio and at position ii the side-to-side coalescence of adjacent loops results in a large loop with its long axis normal to the field instead of the typical parallel configuration.

the director along one line differs in orientation by $\pi/2$ from that along the other line. PLM images of inversion wall loops in an area having a thickness of approximately 0.5−1 μm are shown in Figure 3A, where the magnetic field direction is oriented at 45° to the directions of the polarizer and analyzer. As expected, the wall loops appear as two parallel extinction contours. If the sample is rotated by 45° (Figure 3B) such that the magnetic field direction is now parallel to the polarizer (and perpendicular to the analyzer), the majority of the sample appears dark, as the director is now parallel to the polarizer, the polarization of the incident light is unchanged, and the analyzer extinguishes all light. The sample appears bright only along Néel inversion walls as all distortions in the well-aligned sample are localized to these defects and the director is at some angle to the polarizer. A single dark line appears along the wall centerline. In this region of the wall defect, the director is exactly perpendicular to the magnetic field direction and therefore perpendicular to the polarizer, resulting in an extinction line. Both regular and irregularly shaped inversion wall loops are visible.

The appearance of lamellar-decorated Néel inversion walls at high resolution is demonstrated in Figure 4. AFM images of a Néel bend wall and a Néel splay wall formed in a 13.5 T magnetic field are shown in Figure 4A and B, respectively. These images were taken along straight portions of large loops. Recall that in AFM images of lamellar-decorated polymer liquid crystals, a bend wall in the director field will appear as a splay wall in the lamellae and vice versa, as a result of the orthogonality of the director to the lamellae (see schematic relating lamellar fields to director fields in Figure 4C). Néel bend walls form parallel to the field, where bend is the primary mode of distortion, and Néel splay walls form perpendicular to the field, where splay is the primary mode of distortion.

Early-Stage Development of Néel Inversion Walls. Before the complete 90° reorientation of the director occurs, with inversion walls separating the parallel and antiparallel alignment regions, transient textures develop, where the director is at symmetric intermediate angles to the field on either side of incomplete inversion walls. These transient textures appear under PLM as a periodic pattern of bright and dark lines normal to the applied field direction. PLM images taken after short times in the magnetic field show this texture (Figure 5A). Longberg et al. demonstrated that the wavelength of the periodic structure is dictated by the coupling of reorientation and flow.[22] The period decreases with magnetic field strength and viscosity anisotropy and increases with elastic constants. Rey used numerical analysis to determine that the dynamics of the observed wavelength and final

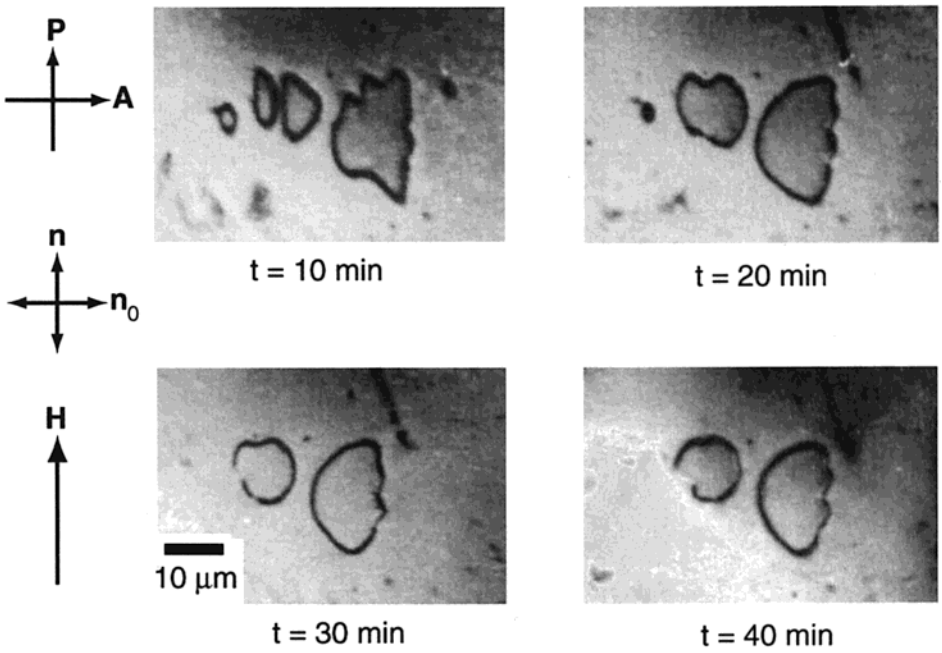

Figure 10. PLM of inversion walls under a 13.5 T magnetic field at 160 °C, showing the evolution of loops with time. The sample is subjected to a series of 10 min increments in the magnetic field while being heated to the liquid crystal regime, with each increment followed by quenching and PLM imaging as appears here. Note the side-by-side coalescence of wall loops in the left side of the micrograph series into one larger wall loop, which subsequently breaks with the resulting $\pm^1/_2$ disclinations moving apart. Smoothing of wall curvature is observed from the first to the second image of the series on the right side. The system energy is lowered by an overall decrease in distortion through a decrease in inversion wall length.

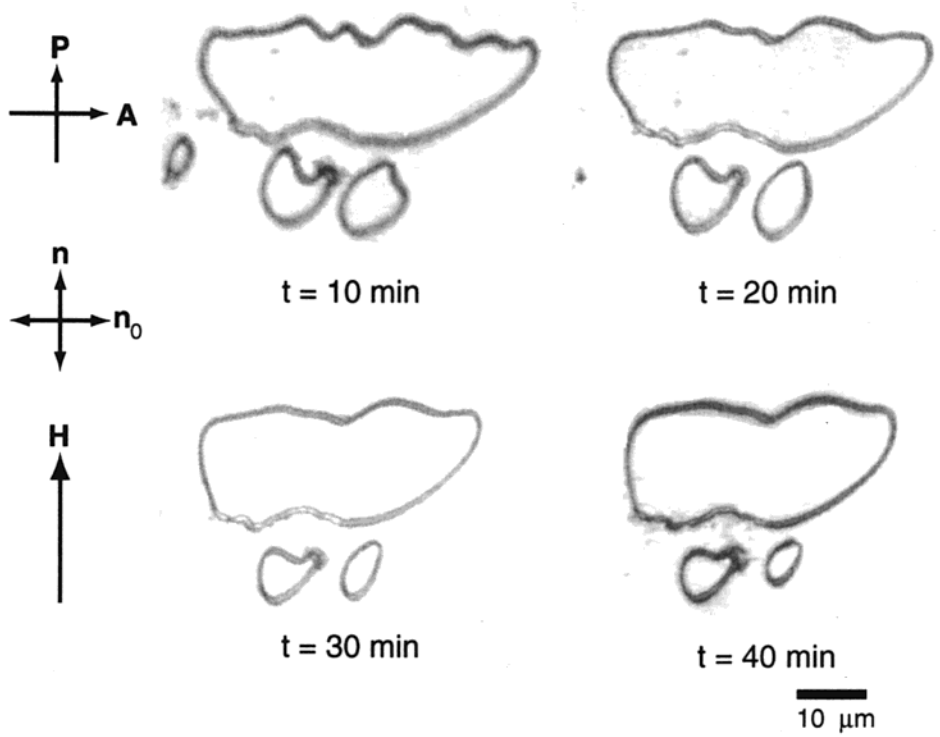

Figure 11. PLM series of a large inversion wall loop under a 13.5 T magnetic field at 160 °C for 10 min intervals. The sample underwent the same treatment as that appearing in the series in Figure 10. The large loop in the top of the image series with its long axis normal to the field likely resulted from the side-by-side coalescence of adjacent wall loops. Note the smoothing of wall curvature along the top length of the loop, again lowering the overall distortion through a decrease in inversion wall length. The small elliptically shaped loop at the bottom right corner of the image series undergoes an overall shrinkage.

polymer orientation are independent of the surface anchoring in the high-field regime.[23] Periodic transient textures were also observed in magnetic field reorientation of thick samples of a lyotropic liquid crystal polymer, poly(*g*-benzyl glutamate), in a solvent mixture of methylene chloride and dioxane by Srajer et al.[24] In these experiments, the low value of k_{22} and the large sample thickness promoted the formation of periodic twist walls parallel to the applied field direction.

Adjacent wall defects can merge and form elongated loops, and these transient loops can evolve into fully formed inversion wall loops as alignment progresses. The incomplete elongated inversion wall loops lie with their long axes parallel to the field. The shape is not a steady-state shape, which is reached at later stages of alignment. Approximately periodically spaced bend wall defects form the sides of the loops, with short portions of energetically costly splay walls at the top and bottom. The top and side portions of two adjacent loops are imaged via high-resolution AFM in Figure 5B. Both types of walls are apparent. The opposing sense of distortion in adjacent periodic walls parallel to the field results in the tops of adjacent loops having distortions of the same sense. (The bottoms of loops have distortions of opposing sense from their tops.)

Magnetic Field Strength Effect. The strength of the magnetic field under which the wall is formed has an influence on its characteristic width, as shown by the AFM images of Néel splay walls in Figure 6. Fully developed inversion walls, with the director undergoing the required 180° rotation between adjacent regions of parallel and antiparallel alignment, were formed in fields of 4, 6, 8, and 13.5 T at 160 °C and quenched after 20 min in the field. These images clearly show that an increase in field strength results in distortion localization with a characteristic width inversely proportional to the applied field strength.

As it is possible to image the director field at high resolution, it is possible to measure the angle the director makes with respect to the field direction as a function of distance from the center of the wall. The characteristic magnetic coherence length, ξ, can then be determined from the equation

$$\phi(x) = 2 \arctan[e^{(\pm \xi/x)}] \tag{12}$$

which gives the angle the director makes with respect to the field direction at a given distance from the center of the wall, $\phi(x)$, where x is the distance from the center of the inversion wall. ξ and ϕ are indicated schematically in Figure 7A.[3] $\phi(x)$ data were fit by the least-squares method to determine a characteristic wall width, ξ, for each field strength. As anticipated, ξ is found to vary approximately linearly with $1/H$. From a plot of ξ versus $1/H$ (Figure 7B), an effective elastic constant, k_{eff}, can be determined from the slope of the plot, because in the equiconstant case

$$\xi = \left(\frac{1}{\mathbf{H}}\right)\left(\frac{\bar{k}_{\text{eff}}}{\chi_a}\right)^{1/2} \tag{13}$$

From our data, we calculate $\bar{k}_{\text{eff}} = 1.6 \times 10^{-6}$ dyn, taking the value of χ_a to be 1.0×10^{-7} emu cgs/g.[25] These data lend support to the numeric model that separates the contributions of splay and bend to the effective elastic constant, yielding a value of $\bar{k}_{ii} = 1.85 \times 10^{-6}$ dyn using values of $k_{11} = 2.8 \times 10^{-6}$ dyn and $k_{33} = 0.9 \times 10^{-6}$ dyn.

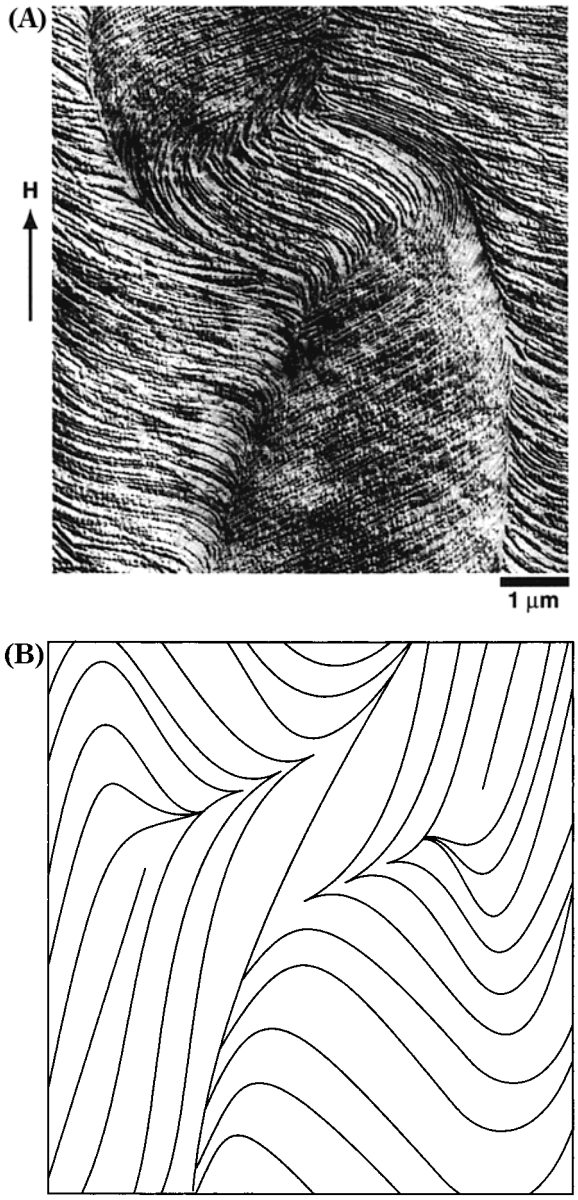

Figure 12. (A) AFM image of two neighboring lamellar-decorated Néel bend walls. (B) Schematic of the orthogonal director pattern of the Néel bend walls shown in Figure 16.

Wall Morphology and Dynamics. A high-resolution SEM image of a small inversion wall loop just under 3 μm in width is shown in Figure 8A. The wall loop transitions continuously from a segment oriented parallel to the field, which appears as a splay wall in the lamellae, indicating a bend wall in the director field, to a segment oriented perpendicular to the field, which appears as a bend wall in the lamellae, indicating a splay wall in the director field. The director in the interior region is at an angle of approximately 15° to that of the exterior director (and the magnetic field), not antiparallel as would be expected. The distortion of the interior is due to the proximity of walls with opposing senses on opposite sides of the small loop. In isolated large inversion wall loops, the directors of both the interior and exterior regions are well-aligned with the magnetic field. As loops shrink and opposite walls approach, the director of the interior region is at some angle to the field. There exists a correlation length-dependent critical wall-to-wall distance below which parallel director alignment with the magnetic field is impossible for the interior. The shrinkage and subsequent disappearance of inversion wall loops in dynamic studies discussed below follows directly. Figure 8B is a schematic of the director field of a wall loop, clearly showing the change in contributions of bend and splay distortions from pure bend distortion in a wall segment oriented parallel to the field to pure splay distortion in a splay wall segment oriented perpendicular to the field.

Wall loops are observed to form with their long axes nearly parallel to the field. Because Néel bend walls form parallel to the field and Néel splay walls form perpendicular to the field, a wall loop with its long axis parallel to the field exhibits more Néel bend wall character than Néel splay wall character. Therefore, even at early stages of observation, it can be inferred that the material favors Néel bend walls, consistent with the values of the splay and bend constants at 160 °C for this polyether.

Loops coalesce, smooth, and shrink anisotropically as alignment improves. Both regularly and irregularly shaped inversion wall loops are observed. Irregularly shaped loops are a result of coalescence of adjacent loops. Both large and small irregularly shaped loops are shown in Figure 9. Wall loops can coalesce top-to-bottom, creating a new loop with an unusually large aspect ratio with the long axis parallel to the field, as in region i in Figure 9, or they can coalesce side-to-side. If multiple loops coalesce side-to-side, a large irregularly shaped inversion wall loop will form with the long axis normal to the field, as in region ii in Figure 9.

The evolution of inversion wall loops at constant magnetic field and temperature was followed by PLM. Figures 10 and 11 show a time lapse series of four PLM images taken after 10 min increments in a 13.5 T field. Side-by-side coalescence of wall loops, loop shrinkage, smoothing of wall curvature, and loop breakage, with the resulting wall-terminating $\pm^1/_2$ disclinations moving apart, are observed. The system energy is lowered by an overall decrease in distortion through a decrease in inversion wall length.

AFM provides high-resolution detail of the coalescence process. Figure 12A shows an AFM image of two neighboring lamellar-decorated Néel wall loops. The orthogonal director pattern is shown schematically in Figure 12B. AFM images point to a coalescence mechanism between adjacent Néel bend walls where opposite-sense inversion walls attract and approach each other and the distortion is replaced by parallel alignment.

The same features can be imaged by both PLM and AFM so that both the size and shape of wall loops, as well as their director fields, can be discerned. Figure 13A is a PLM micrograph of coalescing inversion wall loops. Two loops are captured while coalescing top-to-bottom between adjacent Néel splay walls (at i), while two other loops coalesce side-to-side between adjacent Néel bend walls (ii). The bottom region of the micrograph shows two broken loops (iii). Figure 13B shows a 45-μm^2 field of view AFM image of the coalescing loops imaged by PLM in Figure 13A and surrounding area, with the two pairs of coalescing loops appearing to the left of the image. The upper regions of the loops appear to have already coalesced, and with time, the lower portions of the same walls were observed to annihilate each other as well, leaving behind a well-aligned region. Figure 13C is a 200% enlargement of the area indicated

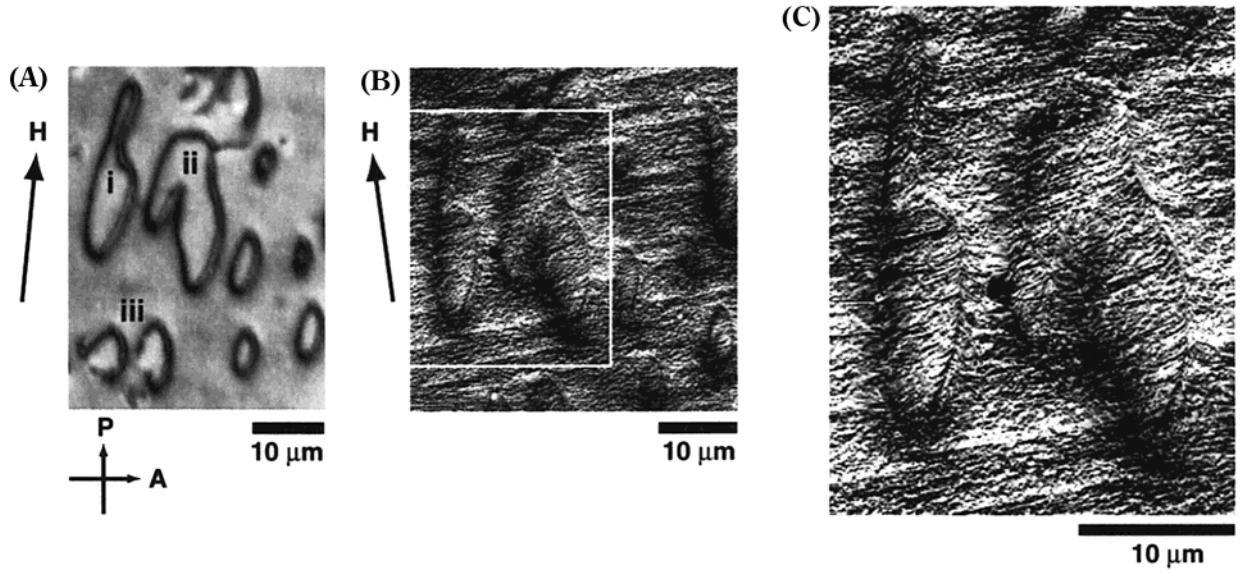

Figure 13. (A) PLM micrograph of coalescing inversion wall loops; in the center left, two loops are captured while coalescing top-to-bottom, and in the center right, two loops are coalescing side-by-side. At the bottom of the micrograph, two broken loops are imaged. The same features can be imaged by both PLM and AFM so that both the size and shape of wall loops, as well as their director fields, can be discerned. (B) AFM image (45 μm^2) of the region at the center of the PLM image in Figure 13A, where the two pairs of coalescing loops appear in the lower left of the image. In the upper region of the micrograph, loops have already coalesced, and with time, the lower portions of the same walls will annihilate each other as well, leaving behind a well aligned region. (C) Enlargement (25 μm^2) of the upper right region of Figure 13B.

in Figure 13B showing the lamellar-decorated director patterns of the top-to-bottom and side-by-side coalescence of these loops. In cases where coalescence of adjacent walls competes with wall shrinkage as a means for minimizing wall distortion, coalescence is more efficient. If adjacent wall loops are spaced closely enough, coalescence occurs; if the loop separation exceeds this critical spacing, the loops will shrink independently.

Because of the Frank elastic constant anisotropy, Néel splay wall segments in this LCP polyether shrink at a faster rate than Néel bend wall segments. Loops shrink anisotropically, with bend wall sections of a loop approaching each other more rapidly, shrinking the length of splay wall sections.

Predictably, the initial sample texture affects the topology of inversion walls observed, and prealignment of the film is important. In the experiments of Hudson and Thomas, the initial state was a schlieren texture in a thermotropic polyester, and Néel bend inversion walls connecting pairs of $\pm 1/2$ strength disclinations were observed after application of a magnetic field.[2] In the present experiments, the initial texture is defect-free, and Néel walls form primarily as continuous inversion wall loops. During later stages of evolution, occasionally a Néel inversion wall terminating in a $+1/2$ disclination at one end and a $-1/2$ disclination at the other is observed. Such features occur when a loop breaks to produce a $\pm 1/2$ disclination line pair, which then proceed initially to move apart as the loop contour shrinks. Figure 14A shows an AFM image of a short Néel splay wall connecting a pair of $\pm 1/2$ disclinations (which is also imaged via PLM in Figure 13A), and Figure 14B presents the corresponding director field. Note that the director field of this wall-terminating $-1/2$ disclination differs from that of a $-1/2$ disclination in an unaligned sample. Distortions are localized closer to the disclination core as a result of the influence of the magnetic field.

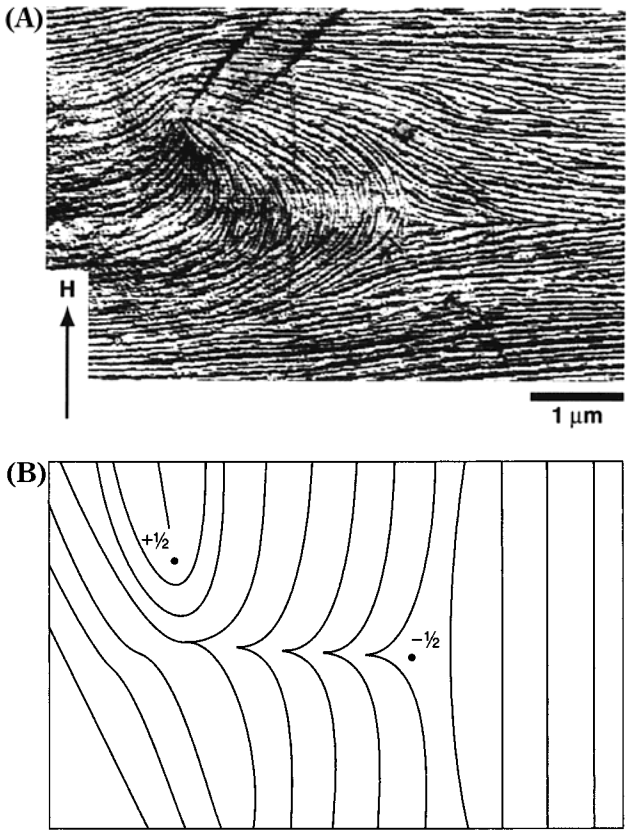

Figure 14. (A) AFM micrograph of a short Néel wall exhibiting both bend character (left) and splay character (right). The wall terminates at one end in a $-1/2$ disclination line and at the other end in a $+1/2$ disclination line. (B) Schematic of the orthogonal director pattern of the Néel wall and its terminating $+1/2$, $-1/2$ disclination line pair shown in Figure 8A. Note that the director field of this wall-terminating $-1/2$ disclination differs from that of a $-1/2$ disclination in an unaligned sample. Distortions are localized closer to the disclination core due to the influence of the magnetic field.

Conclusion

The morphology of metastable inversion walls that developed upon application of a magnetic field to a monodomain of a strongly elastically anisotropic liquid crystal polyether were studied via polarized light microscopy, scanning electron microscopy, and atomic force microscopy. The energies of a Néel bend and a Néel splay wall in an elastically anisotropic nematic within a magnetic field were derived and numerically calculated. For the thermotropic liquid crystal polyether investigated herein, $k_{11} \approx 3k_{33}$, with the energy of the Néel splay wall calculated to be 17% higher than that of Néel bend walls, and thus splay walls are less favored in this system.

Transient textures developed from an initial liquid crystal polymer monodomain during director reorientation, eventually forming Néel bend and Néel splay inversion walls. The lamellar decoration technique allowed for imaging of the director patterns of wall segments at high resolution using scanning electron microscopy and atomic force microscopy. The influence of the aligning magnetic field strength on the characteristic width of alignment distortion is shown by AFM, and the wall width is found to be approximately inversely proportional to the field strength. An effective elastic constant, $\bar{k}_{\text{eff}} = 1.6 \times 10^{-6}$ dyn, was deduced. Primarily, closed inversion wall loops formed, where the inversion wall is continuous and the interior region has antiparallel alignment from the exterior. Loops coalesced, shrank, and smoothed curvature, as well as split into a wall segment terminated by two opposite strength disclinations to reach the new uniform equilibrium state with the director parallel to the applied magnetic field.

Acknowledgment. The authors are grateful for the use of the superconducting magnet facilities at the Francis Bitter Magnet Laboratory, Cambridge, MA, and for the experimental advice and assistance of Dr. Larry Rubin and Dave Lynch. We thank Professor Steve Hudson and Professor Maurice Kléman for useful discussions. This research was supported by AFOSR MURI Grant F49620-97-1-0014 and by NSF-DMR Grant 98-01759.

References and Notes

(1) Frank, F. C. *Discuss. Faraday Soc.* **1958**, *25*, 19.
(2) Hudson, S. D.; Thomas, E. L. *Phys. Rev. A* **1991**, *44*, 8128.
(3) Hudson, S. D.; Vezie, D. L.; Thomas, E. L. *Makromol. Chem., Rapid Commun.* **1990**, *11*, 657.
(4) Ford, J. R.; Bassett, D. C.; Mitchell, G. R.; Ryan, T. G. *Mol. Cryst. Liq. Cryst.* **1990**, *180B*, 233.
(5) Léger, L. *Mol. Cryst. Liq. Cryst.* **1973**, *24*, 33.
(6) Stieb, A.; Baur, G.; Meier, G. *J. Phys.* **1975**, *36*, C1−185.
(7) Helfrich, W. *Phys. Rev. Lett.* **1968**, *21*, 1518.
(8) Thomas, E. L.; Wood, B. A. *Faraday Discuss. Chem Soc.* **1985**, *79*, 229.
(9) Nehring, J.; Saupe, A. *J. Chem. Soc., Faraday Trans. 2* **1972**, *68*, 1.
(10) Mineev, V. P.; Volovik, G. E. *Phys. Rev.* **1978**, *B13*, 3197.
(11) Williams, C.; Vitek, V.; Kléman, M. *Solid State Commun.* **1973**, *12*, 581.
(12) Rey, A. D. *Liq. Cryst.* **1990**, *7*, 315.
(13) Rojstaczer, S.; Stein, R. S. *Mol. Cryst. Liq. Cryst.* **1988**, *157*, 293.
(14) Meyer, R. B. In *Polymer Liquid Crystals*; Ciferri, A., Drigbaum, W. R., Meyer, R. B., Eds.; Academic Press: New York, 1982; p 133.
(15) Mazelet, G.; Kléman, M. *Polymer* **1986**, *27*, 714.
(16) Li, M. H.; Brulet, A.; Davidson, P.; Keller, P.; Cotton, J. P. *Phys. Rev. Lett.* **1993**, *70*, 2297.
(17) Hudson, S. D.; Thomas, E. L. *Phys. Rev. Lett.* **1989**, *62*, 1993,.
(18) Figueiredo Neto, A. M.; Martinot-Lagarde, P.; Durand, G. *J. Phys. Lett.* **1984**, *45*, L-793.
(19) Ding, D.-K.; Thomas, E. L. *Macromolecules* **1993**, *26*, 6531.
(20) Ding, D.-K.; Jin, B.-Y.; Gunther, J.; Thomas, E. L. *Philos. Mag.* **1997**, *76*, 951.
(21) de Gennes, P.-G. *J. Phys.* **1971**, *32*, 789.
(22) Longberg, F.; Fraden, S.; Hurd, A. J.; Meyer, R. E. *Phys. Rev. Lett.* **1984**, *52*, 1903.
(23) Rey, A. D. *Macromolecules* **1991**, *24*, 4450,.
(24) Srajer, G.; Fraden, S.; Meyer, R. B. *Phys. Rev. A* **1989**, *39*, 4828.
(25) Hardouin, F.; Archard, M. F.; Gasparoux, H.; Liebert, L.; Strzelecki, L. J. *J. Polym. Sci. B: Polym. Phys.* **1982**, *165*, 333.

MA010635Y